A Three-Dimensional Thermal Resistance Network Model for Thermal Runaway in Lithium-Ion Batteries

Mohammad Parhizi[1], Jason Ostanek[2], Judith Jeevarajan[1]

1 – Electrochemical Safety Research Institutes
UL Research Institutes
5000 Gulf Fwy, UHTB, Bldg. 4, Rm 138, TX, USA, 77204
Mohammad.Parhizi@ul.org

2 – School of Engineering Technology
Purdue University
401 N. Grant Street, West Lafayette, IN 47907

Abstract

Lithium-ion (Li-ion) batteries have been used widely for various applications, including consumer electronics, electric vehicles, grid storage systems, and military and space applications. However, despite their superior electrochemical characteristics, Li-ion batteries are prone to thermal runaway under certain off-nominal conditions. Under these conditions, Li-ion cells generate excessive amounts of gas and heat, resulting in the venting of flammable gases out of the cell, and causing a potential fire hazard. Modeling and simulation of thermal runaway in Li-ion cells can provide insights into the safe operating limits, help provide guidelines for safer pack/module designs and assist in post-failure diagnostics and analysis. However, modeling thermal runaway in Li-ion cells and batteries is extremely complex due to the multi-physics phenomena involved and the highly nonlinear equations describing them. Thus, systematically reduced-order models are required for specific applications, particularly for scaling up the modeling framework or where a series of simulations must be run. One challenge with reduced-order models is the loss of modeling fidelity that comes with dimensional reduction or simplification of the physical processes. This work presents a series of case studies using a thermal resistance network and lumped mass framework with superior usability that allows creation of complex networks to track heat transfer in all three directions. Due to its simplicity and computational efficiency, the present model can be used for model calibration and parameter estimation (thermophysical properties and kinetic parameters), cell-to-cell variability and statistical analysis, and extending thermal abuse modeling to large battery systems. This presentation will provide examples of some of these practical applications mentioned above and highlights the importance of capturing three-dimensional effects in a thermal resistance network and lumped mass framework.

Keywords

Lithium-Ion Battey, Thermal Runaway, Modeling & Simulation, Thermal Network Model

Introduction

Despite significant advances towards electrification and design improvement of Lithium-ion (Li-ion) batteries, thermal runaway and potential fire hazards are still unsolved issues associated with Li-ion batteries. Consequently, extensive research on thermal runaway has been carried out experimentally and incorporating modeling and simulation techniques. Various modeling frameworks, including lumped capacitance [1], 1-D [2], 2-D axisymmetric [3], and 3-D [4] models, have been used to simulate thermal runaway at the cell level and battery packs. Moreover, a wide range of numerical models with different levels of complexity, from simplified thermal network models [5] up to Computational Fluid Dynamics (CFD-based) models accounting for fluid flow [3] and combustion [6], are available in the literature.

In general, high-fidelity thermal runaway models are extremely complex and computationally expensive due to the highly nonlinear equations describing the multi-physics phenomena involved, a large number of mesh elements, and the small time-step size required for convergence [7]. Reduced-order models, on the other hand, may suffer inaccuracies that come with dimensional reduction or over-simplification of the physical processes. However, reduced-order models are required for scaling up the modeling framework, model calibration, and sensitivity analysis. Thus, a reduced-order model capable of reconstructing the 3-D geometry without many elements is desirable. Current simplified models are primarily based on the concept of lumped mass, which ignores the directional heat transfer entirely. This results in ignoring spatial temperature gradients, lack of capability to account for local phenomena, and limiting the boundary conditions used.

This work develops a 3-D thermal resistance network with excellent versatility, allowing heat transfer calculations in all three dimensions using complex thermal networks and allowing expandability to the module-level. A systematic investigation varying the spatial resolution is conducted and the implications on parameter identification are presented.

Single Cell Thermal Abuse Experiment

The test case considered for the thermal modeling and parameter identification analysis was based on a single 18650 Li-ion cell thermal abuse experiment. The cell was placed in a closed volume chamber, sitting upright on a ceramic tile as shown in Figure 1(a). An axial fan was placed near the top of the chamber to encourage mixing and a baffle was used to protect the fan from ejecta and debris.

The cell was driven to thermal runaway by an external heater having dimensions 25 mm x 25 mm and placed at the midline of the cell, shown in Figure 1(b). The heating power was controlled to maintain a constant 9 °C/min rate of temperature increase. The surface of the cell was instrumented with an array of thermocouples at various axial and circumferential locations, as shown in Figure 1(b) and listed in Table 1. Thermocouple signals were recorded at 1Hz sampling frequency.

Table 1. Thermocouple designations and positions.

Designation	X (mm)	Y (mm)	Z (mm)
TC1	0	32.5	9
TC2	9	32.5	0
TC3	0	32.5	-9
TC2U2	9	55	0
TC4U2	-9	55	0
TC2L2	9	10	0
TC4L2	-9	10	0

Model Framework

The present investigation considers the effect of spatial resolution on parameter identification when using a thermal resistance and lumped mass modeling framework. The thermal model was created using GT-SUITE v2022 for its useability and flexibility in developing system-level models.

A schematic of the modeling approach is shown in Figure 2(a). The 18650 cell is split into two sections: the header and the cell body. The header is modeled as a single, homogeneous, and isotropic material and assigned thermophysical properties of steel. The cell body is modeled as a single, homogeneous material with cylindrical-anisotropic thermal conductivity. The sides and top of the cell were assigned a constant heat transfer coefficient of h = 16 $W \cdot m^{-2} \cdot K^{-1}$ from the air circulation in the enclosure. The bottom of the cell was assigned h_{tile} = 150 $W \cdot m^{-2} \cdot K^{-1}$ representing the combined heat conduction to the tile below the cell and subsequent convection to the air in the enclosure. The initial cell temperature was T_0 = 13.9 °C and the ambient temperature in the enclosure was T_∞ = 16.5 °C.

Table 2. Spatial discretization schemes for the cell body.

Designation (number of thermal masses)	Discretization (number of thermal resistances)
1TM	1 radial 0 circumferential 2 axial
5TM	3 radial 8 circumferential 2 axial
13TM	7 radial 8 circumferential 2 axial
21TM	11 radial 8 circumferential 2 axial

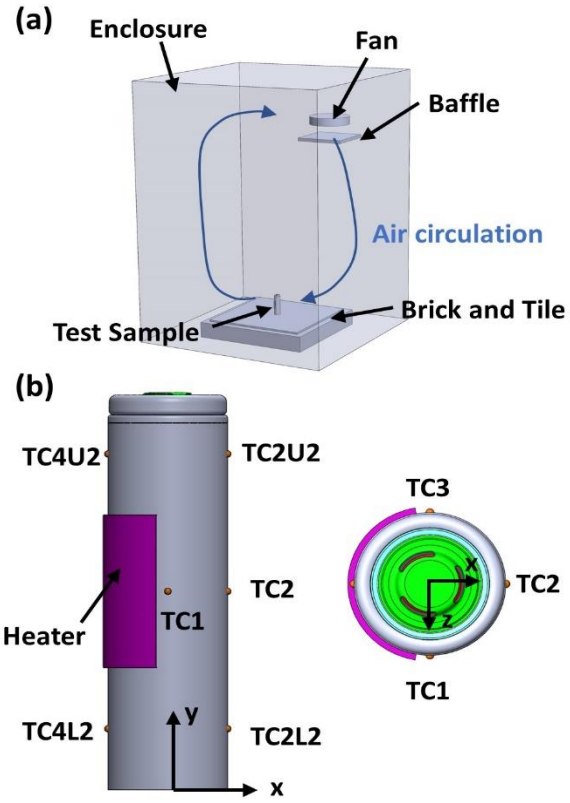

Figure 1. Schematic of experimental apparatus for thermal abuse testing (a) and schematic of instrumented test sample (b).

The cell body was discretized with varying levels of spatial resolution, as shown in Figure 2(b) and Table 2. The model designated "1TM" uses a single thermal mass element, resolves radial conduction with one thermal resistance, and resolves axial conduction with two thermal resistances. The model designated "5TM" uses five thermal masses to capture heat conduction in the circumferential direction and to increase spatial resolution in the radial direction from one to three thermal resistances. The model designated "13TM" increases the spatial resolution to seven thermal resistances in the radial direction and "21TM" further increases the resolution to 11 thermal resistances in the radial direction.

Each thermal mass element in GT-SUITE consists of a thermal node (lumped body) and one or more thermal resistances to allow heat conduction to/from the thermal node. A source heat rate is applied to each thermal mass within the cell body to account for the heat generated from exothermic decomposition reactions. A four-reaction thermal abuse model was used, including reactions for SEI-decomposition, anode-electrolyte reaction, cathode-electrolyte reaction, and electrolyte decomposition [9].

Thermophysical parameter identification was conducted using the optimization tool within GT-SUITE v2022. Table 3 lists the thermophysical parameters, initial values, and allowable range for parameter identification. The accelerated genetic algorithm within GT-SUITE was used for parameter identification.

Table 3. Thermophysical parameter identification.

Parameter	Initial Value	Range
Radial thermal conductivity (k_r)	1 $W \cdot m^{-1} \cdot K^{-1}$	0.1 to 50 $W \cdot m^{-1} \cdot K^{-1}$
Circumferential thermal conductivity (k_θ)	20 $W \cdot m^{-1} \cdot K^{-1}$	0.1 to 50 $W \cdot m^{-1} \cdot K^{-1}$
Axial thermal conductivity (k_θ)	20 $W \cdot m^{-1} \cdot K^{-1}$	0.1 to 50 $W \cdot m^{-1} \cdot K^{-1}$
Specific Heat Capacity (C_p)	1200 $J \cdot kg^{-1} \cdot K^{-1}$	800 to 2000 $J \cdot kg^{-1} \cdot K^{-1}$
Emissivity (ε)	0.8	0.5 to 1.0

Results and Discussion

The thermophysical properties, listed in Table 3, were identified by conducting the non-linear optimization routine over the time range, t = 0 to 1000 s. The identified radial thermal conductivity is shown in Figure 3(a), the identified circumferential and axial thermal conductivity are shown in Figure 3(b), the identified specific heat capacity is shown in Figure 3(c), and the identified surface emissivity is shown in Figure 3(f). The identified parameters show convergence toward expected values as the number of thermal masses increases. For 21TM, the identified parameters were: k_r = 0.43 $W \cdot m^{-1} \cdot K^{-1}$, k_θ = 18.55 $W \cdot m^{-1} \cdot K^{-1}$, k_a = 18.69 $W \cdot m^{-1} \cdot K^{-1}$, C_p = 1168 $J \cdot kg^{-1} \cdot K^{-1}$, and ε = 0.79.

The identified parameters were then transferred from each 3-D thermal resistance model (TM1, TM5, TM13, TM21) to a high-resolution finite volume model (19 x 10^3 volumes, second order spatial discretization, second order implicit time integration). The finite volume had identical geometry, initial conditions, boundary conditions, and material properties as the GT-SUITE optimization model. The experimental and simulated temperatures are compared in Figure 4(a) for 1TM, Figure 4(b) for 5TM, Figure 4(c) for 13 TM, and Figure 4(d) for 21TM. The relatively high radial conductivity identified with the 1TM model resulted in a smaller temperature gradient than the experimental data shown, in Figure 3(a). The 1TM model parameters resulted in an RMSE of 9.6 °C. The lower radial conductivity identified by the 5TM model resulted in a temperature gradient more similar to the experimental data, but the RMSE of 11.4 °C was unimproved relative to the 1TM model. The RMSE of the 5TM model was driven by TC1 and TC3, shown in Figure 1(b), which are directly adjacent to the edge of the heater. Though the 5TM model has increased spatial resolution relative to the 1TM model, the 5TM is still relatively coarse. The heat dissipated by the heater was distributed into the large control volumes and the response of TC1 and TC3 in the model were dampened

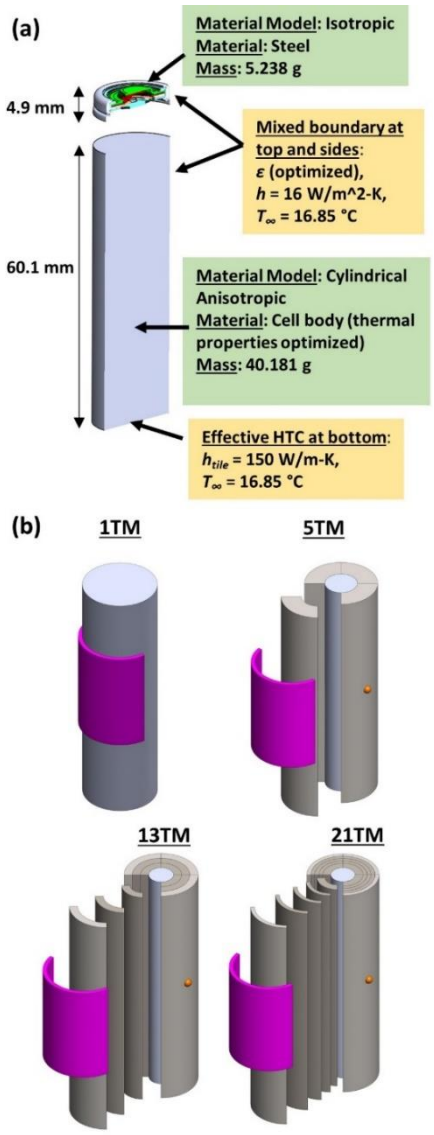

Figure 2. Schematic of geometry, material models, and boundary conditions of numerical model (a) and schematics of four spatial discretization schemes for the cell body (b).

relative to the experiments, leading to an error in the identified thermophysical properties. The same trend continued for 13TM with RMSE of 11.2 °C and 21TM with RMSE of 10.0 °C. The 21TM model is recommended for thermophysical parameter identification and further improvements may be realized by capturing the temperature gradient between the heater and adjacent thermocouples (TC1 and TC3), through increasing spatial resolution in the circumferential direction.

After identifying the thermophysical parameters, each model was used to simulate the full thermal runaway event. Figure 5 compares the temperature of TC2 vs time for each model and experimental data. The 1TM model clearly enters thermal runaway prior to the other models. This implies that

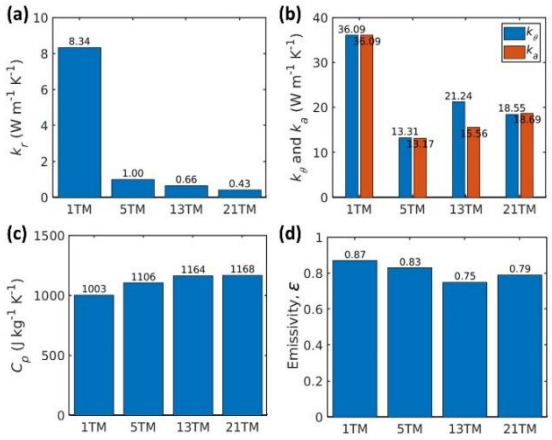

Figure 3. Identified thermophysical properties for 3-D thermal resistance network models of varying degrees of spatial resolution: radial thermal conductivity (a), circumferential and axial thermal conductivity (b), specific heat capacity (c), and emissivity (d).

use of low dimensional models for kinetic parameter identification may produce erroneous results when scaled to high resolution finite volume or finite element models.

Conclusions

A 3-D thermal resistance network with varying degrees of spatial resolution was used to model external heating and thermal abuse of a single, 18650 format cell. The GT-SUITE framework was used due to its built-in optimization tool and scalability to module-level studies. In this work, the built-in optimization tool was used to identify thermophysical and kinetic parameters of decomposition reactions. Parameter identification depends strongly on spatial resolution of the thermal resistance network. Using too few thermal mass elements, particularly in the radial direction, results in errors in thermophysical and kinetic parameters.

References

1. J. K. Ostanek, W. Li, P. P. Mukherjee, K. Crompton, and C. Hacker, "Simulating onset and evolution of thermal runaway in Li-ion cells using a coupled thermal and venting model," *Applied Energy*, vol. 268, 2020.
2. T. Hatchard, D. MacNeil, A. Basu, and J. Dahn, "Thermal model of cylindrical and prismatic lithium-ion cells," *Journal of The Electrochemical Society*, vol. 148, no. 7, p. A755, 2001.
3. J. Kim, A. Mallarapu, D. P. Finegan, and S. Santhanagopalan, "Modeling cell venting and gas-phase reactions in 18650 lithium ion batteries during thermal runaway," *Journal of Power Sources*, vol. 489, 2021.
4. D. Mishra, P. Zhao, and A. Jain, "Thermal Runaway Propagation in Li-ion Battery Packs Due to Combustion of Vent Gases," *Journal of The Electrochemical Society*, vol. 169, no. 10, p. 100520, 2022.
5. Z. Jiang, Z. Qu, J. Zhang, and Z. Rao, "Rapid prediction method for thermal runaway propagation in battery pack based on lumped thermal resistance network and electric circuit analogy," *Applied Energy*, vol. 268, 2020.
6. D. Kong, G. Wang, P. Ping, and J. Wen, "A coupled conjugate heat transfer and CFD model for the thermal runaway evolution and jet fire of 18650 lithium-ion battery under thermal abuse," *E-transportation*, vol. 12, 2022.
7. M. Parhizi, A. Jain, G. Kilaz, and J. K. Ostanek, "Accelerating the numerical solution of thermal runaway in Li-ion batteries," *Journal of Power Sources*, vol. 538, 2022.
8. G. Wang *et al.*, "Modeling venting behavior of lithium-ion batteries during thermal runaway propagation by coupling CFD and thermal resistance network," *Applied Energy*, vol. 334, 2023.
9. Kim et al., "A three-dimensional thermal abuse model for lithium-ion cells," *Journal of Power Sources*, vol. 170, 2007.

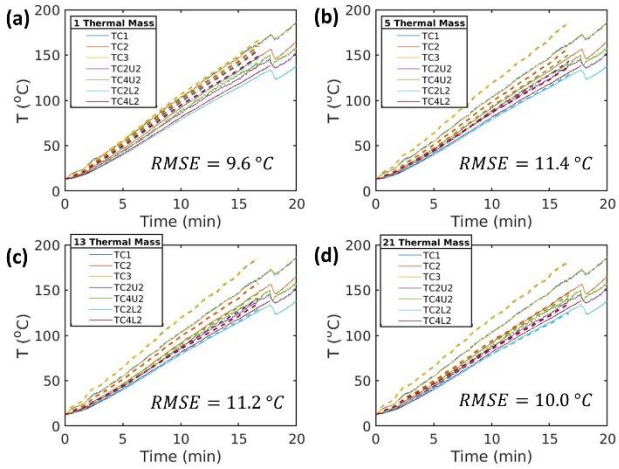

Figure 4. Comparison of high-resolution finite volume simulations (dashed) and experimental temperature vs. time (solid) using parameters identified from the 3-D thermal resistance model: 1TM (a), 5TM (b), 13TM (c), and 21TM (d).

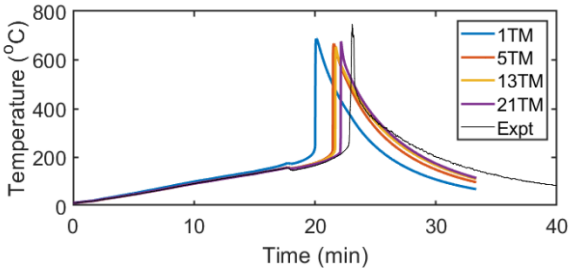

Figure 5. Temperature of TC2 vs. time for each thermal resistance network model and experimental data.